

Dispersive destabilization of nonlinear light propagation in fiber Bragg gratings

Carlos Martel*

*Depto. de Fundamentos Matemáticos,
E.T.S.I. Aeronáuticos, Universidad Politécnica de Madrid,
Plaza Cardenal Cisneros 3, 28040 Madrid, Spain*

Abstract

The effect of retaining the material dispersion terms in the nonlinear coupled mode equations (NLCME) that describe light propagation in fiber Bragg gratings is analyzed. It is found that dispersion is responsible for new instabilities of the uniform states and gives rise to new complex spatio temporal dynamics that is not captured by the standard NLCME formulation. A detailed analysis of the effect of dispersion on the linear stability characteristics of the uniform solutions is presented and some numerical integrations of the NLCME with dispersion are also performed in order to corroborate the theoretical results.

*Electronic address: martel@fmetsia.upm.es

I. INTRODUCTION

The nonlinear coupled mode equations (NLCME) are the envelope equations currently used to study the weakly nonlinear dynamics of light propagation in fiber Bragg gratings. These are universal equations in the sense that they describe the large scale pattern formation of any conservative, spatially extended propagative system with a weak periodic spatial structure. Material dispersion effects are systematically neglected in the derivation that leads to the NLCME. This paper presents a study of the effect of retaining the dispersive terms on the stability of the uniform states and it concludes that these terms should be considered because they give rise to new instabilities and dynamics that are not captured by the NLCME. The NLCME fail, in general, to predict the system evolution and the dispersive terms produce the onset of short scale perturbations that evolve and spread over the domain in the NLCME time scale. Numerical results of the integration of the NLCME with dispersive terms are also provided to corroborate the theoretical linear stability results.

Fiber Bragg gratings (FBG), i.e., optical fibers with a periodic variation of the refractive index along its length, exhibit frequency gaps where light resonates with the periodic structure of the fiber and propagation is not permitted. This frequency dependent reflection characteristic together with the recent developments in grating fabrication techniques has allowed for successful application of FBG in optical communications and fiber sensing, see e.g. [1] for a recent review. Apart from this purely linear effect, the combination of the nonlinearity of the fiber that comes into play at sufficiently high intensities with the spatially distributed reflection produced by the grating gives rise to localized structures known as gap solitons (see [2, 3, 4] and references therein). These gap solitons are solitary waves that, at least in theory, can propagate through the FBG at any speed between zero and the speed of light of the fiber without grating. This possibility of capturing light (gap soliton propagation at zero speed) is currently a topic of great interest because of its promising future applications in the production of devices for optical storage of information.

Light propagation in a nonlinear FBG is usually analyzed using the so-called nonlinear coupled mode equations (NLCME) [2, 5],

$$A_t^+ = v_g A_x^+ + i\Delta n A^- + ig A^+ (\sigma |A^+|^2 + |A^-|^2), \quad (1)$$

$$A_t^- = -v_g A_x^- + i\Delta n A^+ + ig A^- (\sigma |A^-|^2 + |A^+|^2), \quad (2)$$

which prescribe the time (t) evolution along the fiber (x) of the complex envelopes A^+ and A^- of

the wavetrains that resonate with the grating. All variables are assumed to have been previously nondimensionalized in a similar way as in [6], that is, space has been made nondimensional with the grating period λ_g , time with λ_g/c (c is the vacuum speed of light), the grating amplitude with the mean value of the refractive index, and the fields with the characteristic size that results from the Kerr nonlinearity. The actual electric field inside the FBG can be written, in first approximation, as the superposition of two modulated, counterpropagating wavetrains

$$E \sim A^+(x, t) e^{i\pi x + i\omega_0 t} + A^-(x, t) e^{-i\pi x + i\omega_0 t} + \text{c.c.} + \dots, \quad (3)$$

with wavenumber π and frequency $\omega_0 = \omega(k = \pi)$, which is given by the dispersion relation of the fiber without grating $\omega(k)$ (c.c. stands for the complex conjugate). The wavelength of the wavetrains, $\lambda_0 = 2$, is twice the period of the grating, that is assumed to have a spatial profile of the form $\cos(2\pi x)$. This situation can be seen as a spatial parametric resonance that couples both wavetrains: the interaction of one of the wavetrains with the grating gives rise to a resonant term that excites the other wavetrain,

$$\cos(2\pi x) A^+ e^{i\pi x + i\omega_0 t} \sim (e^{i2\pi x} + e^{-i2\pi x}) A^+ e^{i\pi x + i\omega_0 t} \rightarrow A^+ e^{-i\pi x + i\omega_0 t} \quad (A^- \text{ resonant}),$$

and viceversa.

The NLCME take into account the effect of (i) transport at the group velocity, which is given by $v_g = d\omega/dk$ at $k = \pi$, (ii) coupling of the wavetrains through the spatially extended reflection produced by the grating, with Δn proportional to the strength of the grating, and (iii) cubic nonlinear interaction, where $\sigma = \frac{1}{2}$ as a result of the cubic Kerr nonlinearity of the original physical problem for the electric field [2]. The NLCME are also used to describe the evolution of Bose-Einstein condensates in optical lattices [7, 8] and, in general, the NLCME can be regarded as a normal form that applies to any dissipationless propagative system, extended in one spatial dimension, reflection and translation invariant, and with a spatial parametric periodic variation.

The derivation of the NLCME is carried out using a standard multiple scales procedure that requires to assume small amplitudes in (3) with slow spatial and temporal dependence (slow as compared with the wavelength and temporal period of the basic wavetrains), i.e.,

$$\dots \ll |A_{xx}^\pm| \ll |A_x^\pm| \ll |A^\pm| \ll 1, \quad \dots \ll |A_t^\pm| \ll |A^\pm| \ll 1, \quad (4)$$

and small grating intensity,

$$\Delta n \ll 1. \quad (5)$$

The rest of the parameters: ω_0 , v_g and g , are all considered order one quantities. A detailed derivation of the NLCME from the 1D Maxwell-Lorentz equations can be found in [6]. In the process of derivation of the NLCME material dispersion terms ($\sim iA_{xx}^\pm$) are systematically neglected against transport terms ($\sim A_x^\pm$). Notice that this is not the case in the derivation of the nonlinear Schrödinger equation (NLS) for a single modulated wavetrain propagating in an uniform fiber, where both effects are considered because the transport effect can be easily accounted for just by using a moving coordinate frame that travels with the group velocity [9]. If we retain the material dispersion terms, then the resulting equations for A^\pm read

$$A_t^+ = v_g A_x^+ + i d A_{xx}^+ + i \Delta n A^- + i g A^+ (\sigma |A^+|^2 + |A^-|^2), \quad (6)$$

$$A_t^- = -v_g A_x^- + i d A_{xx}^- + i \Delta n A^+ + i g A^- (\sigma |A^-|^2 + |A^+|^2), \quad (7)$$

where $d = -d^2\omega/dk^2$ at $k = \pi$ is the dispersion coefficient that is, generically, an order one quantity. Note that the coefficients of the linear terms of the above envelope equations can be easily obtained from the coefficients of the power expansion of the dispersion relation $\omega(k)$ at $k = \pm\pi$ (see e.g. the review [10]).

In the above equations the transport terms cannot be removed using a moving coordinate transformation and the two effects, transport and dispersion, with different asymptotic orders, see eq. (4), must be considered simultaneously and give rise to two different slow spatial scales:

- a) A transport scale, $\delta x_{\text{trans}} \sim 1/\Delta n \gg 1$, which comes from the balance between the transport along the fiber at the group velocity and the continuous spatial reflection produced by the grating and is the slow spatial scale used in the NLCME derivation [2, 5, 6].
- b) And a dispersive scale, $\delta x_{\text{disp}} \sim 1/\sqrt{\Delta n} \gg 1$, which results from the balance between dispersion and grating reflection. This dispersive scale is small as compared with the transport scale but still large as compared with the basic wavetrain wavelength, i.e.,

$$\delta x_{\text{trans}} \gg \delta x_{\text{disp}} \gg 1,$$

and corresponds to the standard dispersive scaling used in the derivation of the NLS equation [9].

If we look for states exhibiting only transport scales then the dispersion terms in equations (6)-(7) can be neglected in first approximation and these transport dominated solutions are thus well described by the NLCME. But, in general, the question of whether the system will develop dispersive scales or not is a stability question and its answer is not known a priori.

The purpose of the present paper is to demonstrate that the material dispersion terms in eqs. (6)-(7) should not, in general, be neglected because the dispersive scales can be unstable and grow and spread all over the domain. In other words, we will show that stable solutions of the NLCME can be unstable in the context of the more general problem given by eqs. (6)-(7), and can develop dispersive scales that give rise to very complicated spatio-temporal states that are not included in the NLCME description.

To this end, we will consider equations (6)-(7) with simple periodic boundary conditions,

$$A^\pm(x + L, t) = A^\pm(x, t), \quad \text{with } L \gg 1,$$

which correspond to a ring shaped FBG with length L containing an even number of grating periods (like the fiber-loops considered in the simulations of multiple gap soliton collisions in [11]), and we will focus on the effect of dispersion on the stability of the simplest solutions of the NLCME, namely, the solutions with constant uniform modulus. Equations (6)-(7) can be further simplified if we rescale them with the transport scales commonly used for the NLCME [2, 5, 6],

$$\tilde{t} = tv_g/L, \quad \tilde{x} = x/L, \quad \tilde{A}^\pm = \sqrt{gL/v_g} A^\pm, \quad \text{and} \quad \kappa = \Delta n L / v_g, \quad (8)$$

where the scaled grating strength $\kappa \sim 1$, i.e., the FBG length is of the order of the transport scale δx_{trans} . Note that g can always be made positive by making, if necessary, the change of variables $A^\pm \rightarrow \pm A^\pm$ and taking complex conjugates in eqs. (6)-(7). The resulting nonlinear coupled mode equations with dispersion (NLCME_d), after dropping tildes, take the form

$$A_t^+ = -A_x^+ + i\varepsilon A_{xx}^+ + i\kappa A^- + iA^+(\sigma|A^+|^2 + |A^-|^2), \quad (9)$$

$$A_t^- = -A_x^- + i\varepsilon A_{xx}^- + i\kappa A^+ + iA^-(\sigma|A^-|^2 + |A^+|^2), \quad (10)$$

$$A^\pm(x + 1, t) = A^\pm(x, t). \quad (11)$$

where the scaled dispersion $\varepsilon = d/(Lv_g) \ll 1$ and $\kappa \sim 1$, as mentioned above. With this new scaling the transport and dispersive scales are now $\delta x_{\text{trans}} \sim 1$ and $\delta x_{\text{disp}} \sim \sqrt{|\varepsilon|} \ll 1$, and the wavelength of the basic wavetrains in (3) is $\sim |\varepsilon| \ll 1$. The small dispersion term $\varepsilon \ll 1$ in the above equations is essential because it takes into account the fact that we are simultaneously considering two effects, transport and dispersion, that have different asymptotic orders due to the original slow modulation assumption (4). There are some previous works [12, 13, 14] that study the structure and stability of the localized solutions of the NLCME_d (9)-(10), but they all consider $\varepsilon \sim 1$ and do not study the small dispersion limit $\varepsilon \ll 1$, which is the only physically relevant

regime from the point of view of the slow envelope description of the weakly nonlinear light propagation in FBG.

The remainder of this paper is organized as follows. The family of uniform solutions of the NLCME is briefly described in the next section and its linear stability characteristics against perturbations with wavelength $\lambda \sim 1$ (transport scale) and $\lambda \sim \sqrt{|\varepsilon|} \ll 1$ (dispersive scale) are obtained in sections 3 and 4, respectively. These results indicate that the dispersive scales can destabilize the uniform solutions for parameter values where the NLCME predict stability. In the final section, numerical simulations of the NLCMEd with small dispersion are used to corroborate the theoretical stability predictions and some concluding remarks are also drawn.

II. CONTINUOUS WAVES

The constant modulus solutions of the NLCME, also known as continuous waves (CW), can be written as [4, 15]

$$\begin{aligned} A_{\text{cw}}^+ &= \rho \cos \theta e^{i\alpha t + imx}, \\ A_{\text{cw}}^- &= \rho \sin \theta e^{i\alpha t + imx}, \end{aligned}$$

where $\rho > 0$ is the power flowing through the grating, $\theta \in]-\frac{\pi}{2}, 0[\cup]0, \frac{\pi}{2}[$ measures the ratio between the two counterpropagating wavetrains, and α and m are given by

$$\begin{aligned} \alpha &= \frac{\kappa}{\sin 2\theta} + \frac{1 + \sigma}{2} \rho, \\ m &= \left(\frac{\kappa}{\sin 2\theta} + \frac{1 - \sigma}{2} \rho^2 \right) \cos 2\theta. \end{aligned}$$

According to eq. (3), the associated electric field inside the grating consists of the superposition of two uniform wavetrains, and α and m represent small corrections to the frequency and wavenumber of the wavetrains. The resulting pattern resembles a standing wave for θ near $\pm\frac{\pi}{4}$ and a traveling wave for θ close to 0 and $\pm\frac{\pi}{2}$.

In the linear limit of small light intensity, $\rho \rightarrow 0$, the relation between the frequency, α , and the wavenumber, m , of the CW takes the form

$$m^2 = \alpha^2 \left(1 - \frac{\kappa^2}{\alpha^2} \right),$$

which is plotted in Fig. 1 and shows a frequency gap of size 2κ where light propagation is not allowed (this is a typical resonance effect in wave propagation in periodic media). As the power

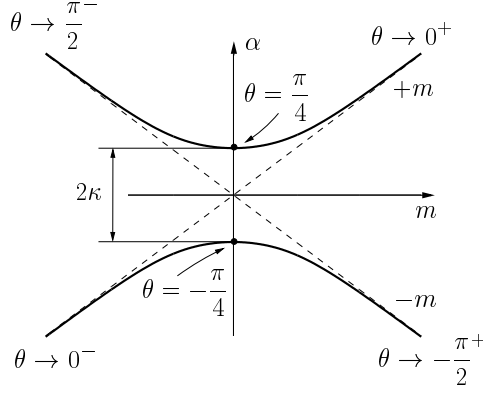


Figure 1: $\alpha - m$ plot of the CW in the linear regime $\rho \rightarrow 0$.

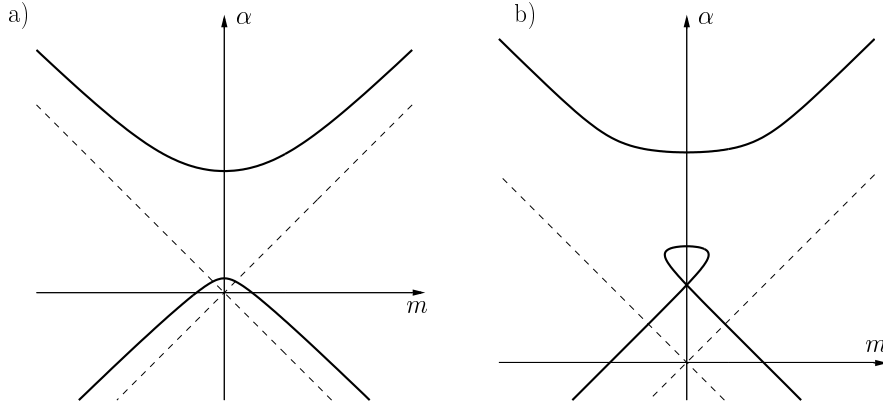


Figure 2: $\alpha - m$ plot of the CW for a) $\rho < \rho_c$ and b) $\rho > \rho_c$ ($\sigma = \frac{1}{2}$).

is increased, the nonlinearity of the problem comes into play and the relation between α and m becomes more involved

$$m^2 = (\alpha - \sigma \rho^2)^2 \left(1 - \frac{\kappa^2}{(\alpha - (\frac{1+\sigma}{2})\rho^2)^2}\right).$$

There are still two CW for any given m if $\rho^2 < \rho_c^2 = 2\kappa/(1 - \sigma)$, see Fig. 2a, while for $\rho^2 > \rho_c^2$ a region of higher multiplicity of solutions (up to 4) develops near $m = 0$ [4], as it can be appreciated from Fig. 2b. Notice that the frequency gap persists for $\rho > 0$ and it remains of size 2κ but it is shifted upwards by the nonlinear effects.

In the rest of this paper the family of the CW is going to be represented in the (θ, ρ^2) plane shown in Fig. 3. The CW inside the region marked by thick line

$$\rho^2 = \rho_x^2 = -\frac{2\kappa}{(1 - \sigma) \sin(2\theta)} \quad (12)$$

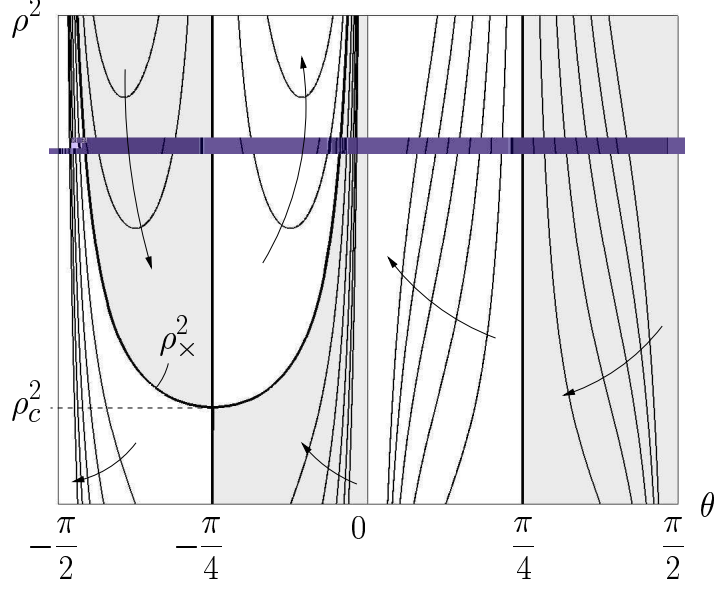


Figure 3: (θ, ρ^2) representation of the CW ($\sigma = \frac{1}{2}$).

are those along the loop in Fig. 2b. The wavenumber m is positive (negative) in the white (shaded) areas and the thin lines correspond to the values of the wavenumber compatible with the periodicity boundary conditions (11), $m = 2\pi n$ with $n \in \mathbb{Z}$ (arrows indicate the m increasing direction). Note that the $\theta = \pm \frac{\pi}{4}$ symmetry is due to the fact that the CW associated with $\theta > 0$ ($\theta < 0$) and $\frac{\pi}{2} - \theta$ ($-\frac{\pi}{2} - \theta$) are essentially the same after applying the spatial reflection symmetry of the system $x \rightarrow -x$ and $A^+ \leftrightarrow A^-$,

III. CW STABILITY: TRANSPORT SCALE PERTURBATIONS

The CW are approximate solutions (up to order ε corrections) of the NLCMED and its infinitesimal perturbations

$$A^+ = A_{\text{cw}}^+(1 + a^+), \quad A^- = A_{\text{cw}}^-(1 + a^-), \quad \text{with } |a^\pm| \ll 1,$$

evolve according to the linearized version of the NLCMED

$$a_t^+ - a_x^+ = i\kappa(a^- - a^+) \tan \theta + i\sigma\rho^2 \cos^2 \theta (a^+ + \overline{a^+}) + i\rho^2 \sin^2 \theta (a^- + \overline{a^-}) + i\varepsilon a_{xx}^+, \quad (13)$$

$$a_t^- + a_x^- = i\kappa(a^+ - a^-) / \tan \theta + i\sigma\rho^2 \sin^2 \theta (a^- + \overline{a^-}) + i\rho^2 \cos^2 \theta (a^+ + \overline{a^+}) + i\varepsilon a_{xx}^-, \quad (14)$$

$$a^\pm(x+1, t) = a^\pm(x, t), \quad (15)$$

which, by means of the spatial Fourier expansion

$$(a^+, a^-) = \sum_{k=-\infty}^{\infty} (a_k^+(t), a_k^-(t)) e^{i2\pi kx},$$

can be turned into a system of ordinary differential equations of the form

$$\begin{aligned} \frac{da_k^+}{dt} = & i(2\pi k)a_k^+ + i\kappa(a_k^- - a_k^+) \tan \theta + i\sigma\rho^2 \cos^2 \theta (a_k^+ + \overline{a_{-k}^+}) \\ & + i\rho \sin^2 \theta (a_k^- + \overline{a_{-k}^-}) - i\varepsilon(2\pi k)^2 a_k^+, \end{aligned} \quad (16)$$

$$\begin{aligned} \frac{da_k^-}{dt} = & -i(2\pi k)a_k^- + i\kappa(a_k^+ - a_k^-) / \tan \theta + i\sigma\rho^2 \sin^2 \theta (a_k^- + \overline{a_{-k}^-}) \\ & + i\rho^2 \cos^2 \theta (a_k^+ + \overline{a_{-k}^+}) - i\varepsilon(2\pi k)^2 a_k^-, \end{aligned} \quad (17)$$

where $k \in \mathbb{Z}$ indicates the wavenumber of the perturbation.

Perturbations with wavelength of the order of the transport scale have wavenumbers $k \sim 1$ and for them the dispersion terms $i\varepsilon(2\pi k)^2 a_k^\pm$ in the equations above are small and can be neglected in first approximation. The resulting equations for a_k^\pm together with those corresponding to $\overline{a_{-k}^\pm}$ form a linear quartet uncoupled from the rest whose solutions are of the form

$$(a_k^\pm(t), \overline{a_{-k}^\pm(t)}) = (a_k^{0\pm}, \overline{a_{-k}^{0\pm}}) e^{i\omega t}, \quad (18)$$

where ω is given by the following fourth order polynomial with real coefficients

$$\begin{aligned} (\omega^2 - (2\pi k)^2)^2 - 2\kappa^2(\omega^2 - (2\pi k)^2) + 4\kappa\rho^2 \frac{\tan \theta}{1 + \tan^2 \theta} ((2\pi k)^2(1 + \sigma) - \omega^2(1 - \sigma)) \\ - \kappa^2 \tan^2 \theta (\omega + (2\pi k))^2 - \frac{\kappa^2}{\tan^2 \theta} (\omega - (2\pi k))^2 = 0. \end{aligned} \quad (19)$$

This polynomial results from the NLCME, that is, when dispersion is not considered, and it was previously analyzed in [15] for some particular values of ρ^2 and θ . In this section we will complete these results and give a detailed description of the CW instability regions given by (19).

For the particular case of uniform perturbations, $k = 0$, the solutions of (19) can be calculated explicitly

$$\omega = \pm \sqrt{\frac{4\kappa^2}{\sin^2(2\theta)} + 2\kappa\rho^2(1 - \sigma) \sin(2\theta)}, \quad \omega = 0 \text{ (double) and}$$

and we have instability, i.e., ω with negative imaginary part, when

$$\rho^2 > \rho_0^2 = -\frac{2\kappa}{(1 - \sigma) \sin^3(2\theta)}. \quad (20)$$

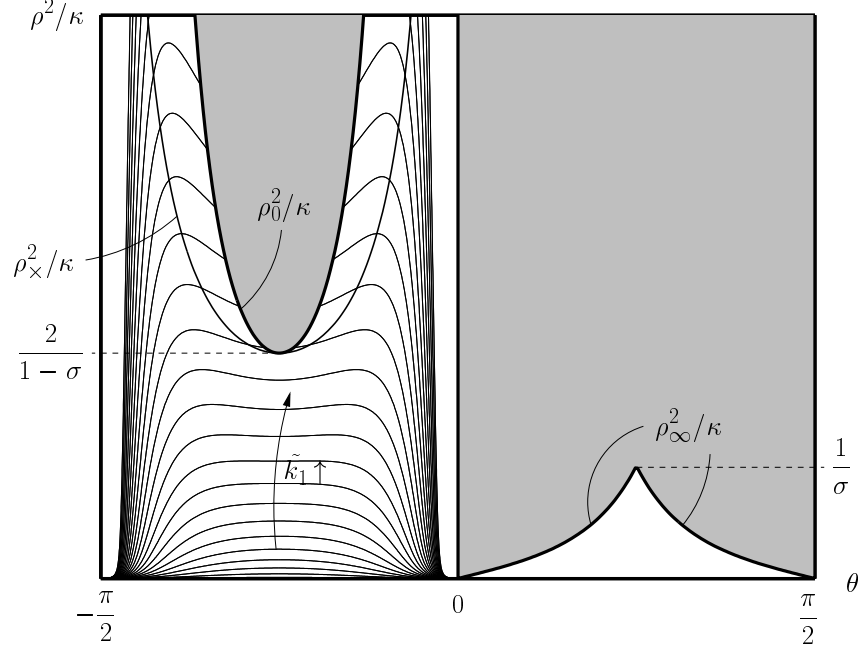


Figure 4: CW stability properties ($\sigma = \frac{1}{2}$). Shading indicates instability and the thin lines correspond to $\tilde{k}_1 = 0.25 + 0.25n$, with $n = 0, 1, 2, \dots$. The CW above the $\tilde{k}_1 = 2\pi/\kappa$ line are unstable, see eq. (23).

This instability region lies inside the higher multiplicity region given by eq. (12), see Fig. 4, and it destabilizes the CW on the upper part of the loop in Fig. 2b.

In the limit of large wavenumbers, $k \rightarrow \pm\infty$, the solutions of eq. (19) can be expanded as

$$\omega = \omega_0 + \omega_1 + \dots, \quad \text{with} \quad |\omega_0| \gg |\omega_1| \gg \dots$$

The first order term $\omega_0 \sim k \gg 1$ satisfies the equation

$$(\omega_0^2 - (2\pi k)^2)^2 = 0,$$

whose solutions are of the form $\omega_0 = \pm 2\pi k$ and represent pure oscillations. The next order correction $\omega_1 \sim 1$ is given by

$$\omega_1^2 = \kappa^2 \tan^{\pm 2} \theta - 2\sigma\kappa\rho^2 \frac{\tan \theta}{1 + \tan^2 \theta}$$

and the CW are therefore unstable inside the region defined by the conditions

$$\rho^2 > \rho_\infty^2 = \frac{\kappa \tan^{\pm 2} \theta}{\sigma \sin(2\theta)}, \quad (21)$$

which is plotted in Fig. 4. Notice that, for the CW in this region, all perturbations with wavenumber above a given one are unstable. This unphysical behavior (amplification of perturbations far

away from the Bragg resonance) was already detected in [15] where it was suggested that it could be fixed by the addition dispersion. This affirmation is true, as it will be seen in the next section where the stability of perturbations with high wavenumbers is analyzed.

The localization of the unstable perturbations with finite nonzero wavenumber $0 < |k| < \infty$ requires to numerically explore the roots of (19) and can be simplified by taking into account the invariance of eq. (19) under the transformations

$$(\omega, k) \rightarrow (-\omega, -k) \quad \text{and} \quad (\omega, \tan \theta) \rightarrow (-\omega, 1/\tan \theta)$$

that allows us to restrict the search to the parameter range

$$k > 0 \quad \text{and} \quad \theta \in [-\frac{\pi}{4}, \frac{\pi}{4}].$$

Furthermore, if we use the scaled variables

$$\tilde{\omega} = \omega/\kappa, \quad \tilde{k} = (2\pi k)/\kappa \quad \text{and} \quad \tilde{\rho}^2 = \rho^2/\kappa, \quad (22)$$

then the strength of the grating, $\kappa > 0$, can be absorbed and eq. (19) can be rewritten as

$$\begin{aligned} (\tilde{\omega}^2 - \tilde{k}^2)^2 - 2(\tilde{\omega}^2 - \tilde{k}^2) + 4\tilde{\rho}^2 \frac{\tan \theta}{1 + \tan^2 \theta} (\tilde{k}^2(1 + \sigma) - \tilde{\omega}^2(1 - \sigma)) \\ - \tan^2 \theta (\tilde{\omega} + \tilde{k})^2 - \frac{1}{\tan^2 \theta} (\tilde{\omega} - \tilde{k})^2 = 0. \end{aligned}$$

The onset of complex roots (instability) takes place when both the equation above and its derivative with respect to $\tilde{\omega}$ vanish. From these two conditions the values of θ and $\tilde{\rho}^2$ can be numerically computed for any given $\tilde{\omega}$ and \tilde{k} , and the following results are obtained:

- If $\theta > 0$ then there are no more instabilities apart from the one already obtained for $k \rightarrow \pm\infty$ (21), see Fig. 4.
- For each negative θ and for each value of $\tilde{\rho}^2 = \rho^2/\kappa$ there is a critical scaled wavenumber \tilde{k}_1 such that the perturbations with $0 < \tilde{k} < \tilde{k}_1$ are unstable and those with $\tilde{k} > \tilde{k}_1$ are stable (constant \tilde{k}_1 curves are plotted as thin solid lines in Fig. 4). A CW will be then unstable if the perturbation mode with lowest wavenumber ($k = 1$) is unstable, that is, if

$$\frac{2\pi}{\kappa} < \tilde{k}_1, \quad (23)$$

recall the definition of \tilde{k} in (22). For a given value of κ , all the CW above the line $\tilde{k}_1 = 2\pi/\kappa$ in Fig. 4 are unstable.

- The CW near the $\rho^2 = \rho_0^2$ line exhibit a small interval of stable scaled wavenumbers $\tilde{k} \in [0, \tilde{k}_2]$ with $\tilde{k}_2 < \tilde{k}_1$, but, as it has been checked numerically, this does not modify the instability region defined above.

The complete stability characteristics of the CW against transport scale perturbations (which are accurately described by the NLCME) are summarized in Fig.4. There are three instability boundaries that mark the destabilization of the uniform perturbations (20), high wavenumber perturbations (21) and perturbations with wavenumber $k = 1$ (23). The two first instability conditions are not sensitive to the FBG length and depend only on the combination ρ^2/κ while the third one depends also on κ and it accounts for the stabilizing effect of the finite size of the domain; in an infinite FBG ($\kappa \rightarrow \infty$, see the last eq. in (8)) all CW with $\theta < 0$ are unstable due to (23).

IV. CW STABILITY: DISPERSIVE SCALE PERTURBATIONS

The CW perturbations with wavelength of the order of the dispersive scale have large wavenumbers, $k \sim 1/\sqrt{|\varepsilon|} \gg 1$, and for them the dispersion terms in eqs. (16)-(17) can not be neglected. In order to study the stability of these perturbations, we define the scaled wavenumber $K = (2\pi k)\sqrt{|\varepsilon|} \sim 1$ and expand the solution of eqs. (16)-(17) in the form

$$a_K^+ = a_{K0}^+(t, T) + \sqrt{|\varepsilon|} a_{K1}^+(t, T) + \dots, \quad a_K^- = a_{K0}^-(t, T) + \sqrt{|\varepsilon|} a_{K1}^-(t, T) + \dots,$$

where $T = t/\sqrt{|\varepsilon|}$ is a fast time scale. At first order we obtain

$$\begin{aligned} \frac{da_{K0}^+}{dT} - iK a_{K0}^+ &= 0, \\ \frac{da_{K0}^-}{dT} + iK a_{K0}^- &= 0, \end{aligned}$$

whose general solution is given by

$$(a_{K0}^+, a_{K0}^-) = (A_{K0}^+(t) e^{iKT}, A_{K0}^-(t) e^{-iKT}).$$

Thus, in the fast time scale T , the group velocity term dominates and these narrow dispersive perturbations simply travel in opposite directions. At next order we obtain

$$\begin{aligned} \frac{da_{K1}^+}{dT} - iK a_{K1}^+ &= \left[-\frac{dA_{K0}^+}{dt} - i(\kappa \tan \theta + \frac{\varepsilon}{|\varepsilon|} K^2) A_{K0}^+ + i\sigma \rho^2 \cos^2 \theta (A_{K0}^+ + \overline{A_{K0}^+}) \right] e^{iKT} \\ &\quad + [i\kappa \tan \theta A_{K0}^- + i\rho^2 \sin^2 \theta (A_{K0}^- + \overline{A_{K0}^-})] e^{-iKT}, \\ \frac{da_{K1}^-}{dT} + iK a_{K1}^- &= \left[-\frac{dA_{K0}^-}{dt} - i(\kappa / \tan \theta + \frac{\varepsilon}{|\varepsilon|} K^2) A_{K0}^- + i\sigma \rho^2 \sin^2 \theta (A_{K0}^- + \overline{A_{K0}^-}) \right] e^{-iKT} \\ &\quad + [i\kappa / \tan \theta A_{K0}^+ + i\rho^2 \cos^2 \theta (A_{K0}^+ + \overline{A_{K0}^+})] e^{iKT}, \end{aligned}$$

and the higher order correction (a_{K1}^+, a_{K1}^-) will then remain bounded in the fast time scale T if the following equations are satisfied

$$\frac{dA_{K0}^+}{dt} = -i(\kappa \tan \theta + \frac{\varepsilon}{|\varepsilon|} K^2) A_{K0}^+ + i\sigma \rho^2 \cos^2 \theta (A_{K0}^+ + \overline{A_{K0}^+}), \quad (24)$$

$$\frac{dA_{K0}^-}{dt} = -i(\kappa / \tan \theta + \frac{\varepsilon}{|\varepsilon|} K^2) A_{K0}^- + i\sigma \rho^2 \sin^2 \theta (A_{K0}^- + \overline{A_{K0}^-}), \quad (25)$$

which give the evolution of A_{K0}^\pm in the slow time scale t . The left (+) and right (-) propagating perturbations are not coupled, and the equations above together with the corresponding ones for $\overline{A_{K0}^+}$ and $\overline{A_{K0}^-}$ form two linear systems with constant coefficients whose solutions are proportional to $e^{\Omega^\pm t}$, with

$$\Omega^+ = \pm \sqrt{(\kappa \tan \theta + \frac{\varepsilon}{|\varepsilon|} K^2)(2\sigma \rho^2 \cos^2 \theta - (\kappa \tan \theta + \frac{\varepsilon}{|\varepsilon|} K^2))} \quad \text{and} \quad (26)$$

$$\Omega^- = \pm \sqrt{(\kappa / \tan \theta + \frac{\varepsilon}{|\varepsilon|} K^2)(2\sigma \rho^2 \sin^2 \theta - (\kappa / \tan \theta + \frac{\varepsilon}{|\varepsilon|} K^2))}. \quad (27)$$

The dispersive perturbations are then unstable if the following conditions are satisfied

$$\begin{aligned} 0 &\leq \kappa \tan \theta + \frac{\varepsilon}{|\varepsilon|} K^2 \leq 2\sigma \rho^2 \cos^2 \theta, \\ 0 &\leq \kappa / \tan \theta + \frac{\varepsilon}{|\varepsilon|} K^2 \leq 2\sigma \rho^2 \sin^2 \theta, \end{aligned}$$

that can be expressed as

$$\rho^2 \geq \rho_+^2 = \frac{\tan \theta}{\sigma \sin(2\theta)} (\kappa \tan \theta + \frac{\varepsilon}{|\varepsilon|} K^2) \quad \text{with} \quad \tan \theta \geq \frac{\varepsilon}{|\varepsilon|} \frac{K^2}{\kappa}, \quad (28)$$

$$\rho^2 \geq \rho_-^2 = \frac{\tan^{-1} \theta}{\sigma \sin(2\theta)} (\kappa \tan^{-1} \theta + \frac{\varepsilon}{|\varepsilon|} K^2) \quad \text{with} \quad \tan^{-1} \theta \geq \frac{\varepsilon}{|\varepsilon|} \frac{K^2}{\kappa}. \quad (29)$$

Notice that if we set $K^2 = 0$ in the equations above then the instability condition given by eq. (21) is recovered, in other words, the limit $k \rightarrow \pm\infty$ for the $k \sim 1$ (transport scale) regime matches with the limit $K \rightarrow 0$ for the $k \sim 1/\sqrt{|\varepsilon|} \gg 1$ (dispersive scale) regime.

The above instability conditions depend on the parameter $K^2 > 0$ and define two families of regions in the (θ, ρ^2) plane, which are represented in Fig.5 for $\varepsilon > 0$ and several values of $K^2 > 0$ (note that expression (28) is identical to (29) if we change $\tan \theta$ by $1/\tan \theta$ and therefore the instability region defined by the ρ_-^2 condition is simply the symmetric of that defined by ρ_+^2 around the vertical axes $\theta = \pm \frac{\pi}{4}$). A variation of the wavenumber from k to $k+1$ results in a very small increment of the scaled wavenumber $\Delta K \sim \sqrt{|\varepsilon|} \ll 1$, so, in first approximation, we have to allow K^2 to vary continuously between 0 and $+\infty$ in (28)-(29). The resulting final dispersive

instability region is then given by the union of all these K^2 dependent regions. All CW with θ negative are thus rendered unstable for $\varepsilon > 0$ (see Fig.5) and, in a completely similar way, if $\varepsilon < 0$ then all the CW with positive θ are unstable (see Fig.6).

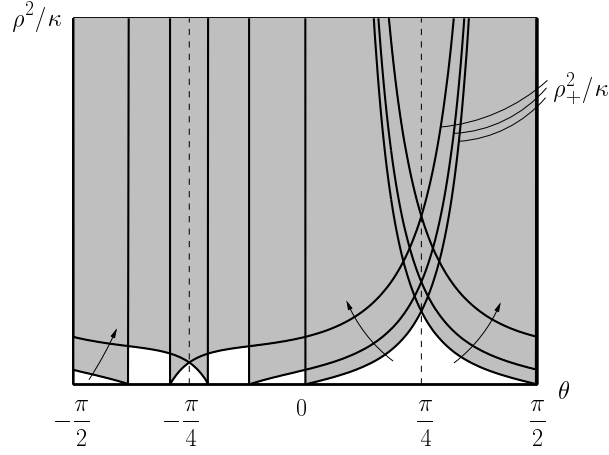


Figure 5: Dispersive instability regions defined by eqs. (28) and (29) for $\varepsilon > 0$ and three different values of K^2 , with arrows pointing towards increasing K^2 direction and shading indicating instability ($\sigma = \frac{1}{2}$).

Therefore, the CW stability diagram represented in Fig.4 has to be complemented with the following dispersive instability criterion:

$$- \text{ for } \varepsilon > 0 \text{ (} \varepsilon < 0 \text{), all CW with } \theta < 0 \text{ (} \theta > 0 \text{) are unstable,} \quad (30)$$

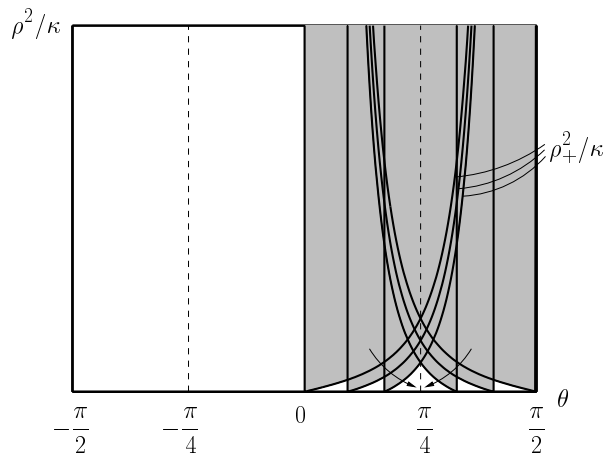


Figure 6: Dispersive instability regions defined by eqs. (28) and (29) for $\varepsilon < 0$ and three different values of K^2 , with arrows pointing towards increasing K^2 direction and shading indicating instability ($\sigma = \frac{1}{2}$).

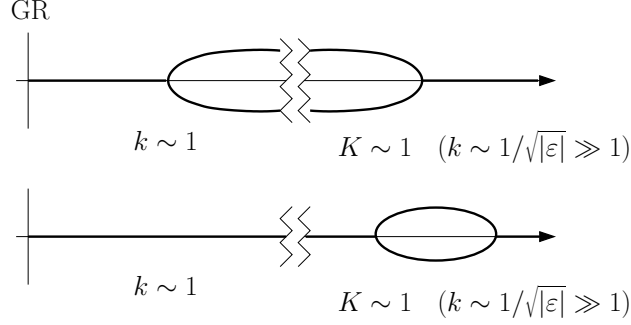


Figure 7: Sketch of the maximum growth rate of the transport and dispersive perturbations as a function of the wavenumber

which states that all the CW along the lower (upper) branch in Fig.2 are unstable if ε is positive (negative).

As it was advanced in [15], the material dispersion corrects the unphysical high wavenumber instability found in the previous section, see eqs. (26) and (27) and the upper plot in Fig.7. But it also gives rise to new instabilities (lower plot of Fig.7) that are not detected if the NLCME description is used and that are present independently of the dispersion sign: according to (30), positive (negative) dispersion is responsible for the destabilization of NLCME stable CW with $\theta < 0$ ($\theta > 0$) in the lower part of Fig.2. These high wavenumber dispersive perturbations travel with the group velocity and their growth rate remain of order unity as $\varepsilon \rightarrow 0$, see eqs. (26)-(27), i.e., they evolve in the transport time scale $t \sim 1$.

V. DISCUSSION AND CONCLUSIONS

As a final check of the theoretical dispersive instability results obtained in the previous section, several numerical simulations of the NLCMEd have been performed for the two cases shown in Fig.8 with different dispersion coefficients. The numerical method uses a Fourier series in space with N_{Fourier} modes and a 4th order Runge-Kutta scheme for the time integration of the resulting system of ODEs, with the linear diagonal terms integrated implicitly and the nonlinear terms computed in physical space using the 2/3 rule to remove the aliasing terms [16] (typical required resolutions were in the range $N_F = 256, \dots, 1024$ and $\Delta t = .01, \dots, .001$).

The CW1 is stable in the NLCME context (i.e., stable against transport scale perturbations) and according to the dispersive instability criterion (30) is also stable for negative values of the disper-

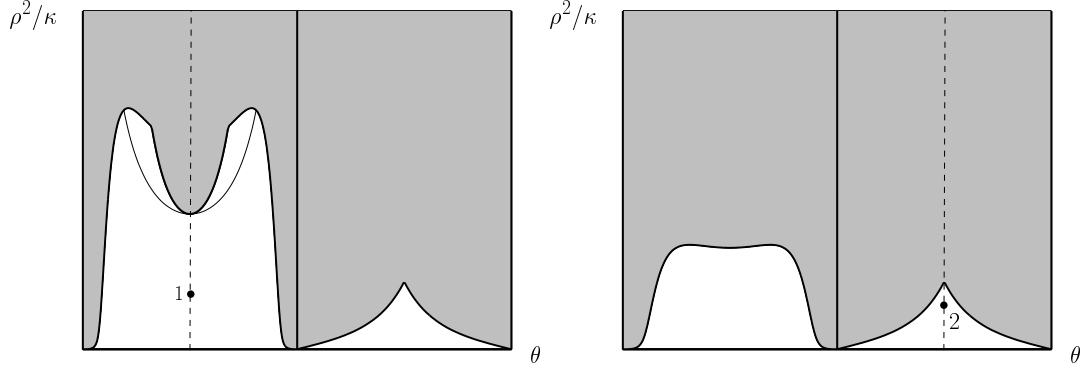


Figure 8: CW stability properties for $\kappa = 1$ and $\kappa = 2$, with shading indicating instability (dispersive instabilities not shown) and dots corresponding to CW1: $\kappa = 1$, $\rho^2 = 1$, $\theta = -\frac{\pi}{4}$, and CW2: $\kappa = 2$, $\rho^2 = 2$, $\theta = \frac{\pi}{4}$ ($\sigma = \frac{1}{2}$).

sion. This is corroborated by the numerical results presented in Fig.9, where the time evolution of the spatial norm of the amplitudes and its derivatives,

$$\|f\| = \sqrt{\int_0^1 |f|^2 dx},$$

is plotted for $\varepsilon = -10^{-3}$. The CW1 remains stable and the small initial perturbation does not grow. Note that the perturbation cannot decay to zero because of the absence of dissipation in the system, and thus the value of the spatial derivatives remains finite but small (comparable to the size of the initial perturbation, see Fig.9). In contrast, if dispersion is positive, the CW1 is unstable due to the exponential amplification of the small dispersive scales, see Fig.10. This growth is not a slow time effect; it takes place in the time scale $t \sim 1$ and does not vanish as $\varepsilon \rightarrow 0$, as it can be seen in the lower plot in Fig.10, where the evolution of the spatial derivatives for two smaller dispersion values has been added for comparison. The solution that develops is shown in Fig.11 and it consists of two counter-propagating wavetrains with dispersive wavelength ($\sim \sqrt{\varepsilon} \ll 1$) moving at the group velocity; notice how the number of peaks is approximately doubled when the dispersion is divided by 4.

For the CW2 in Fig. 8 the situation is the opposite of that of the CW1. Now the CW2 is stable for positive values of the dispersion (the time evolution plot of the norms is omitted in this stable case because it is identical to that shown in Fig.9) and the dispersive instability develops, producing small dispersive scales all over the domain, for negative dispersion, see Fig.12. The time plot of $\|A_x^\pm\|$ in Fig.12 shows the development of the dispersive instability for several dispersion

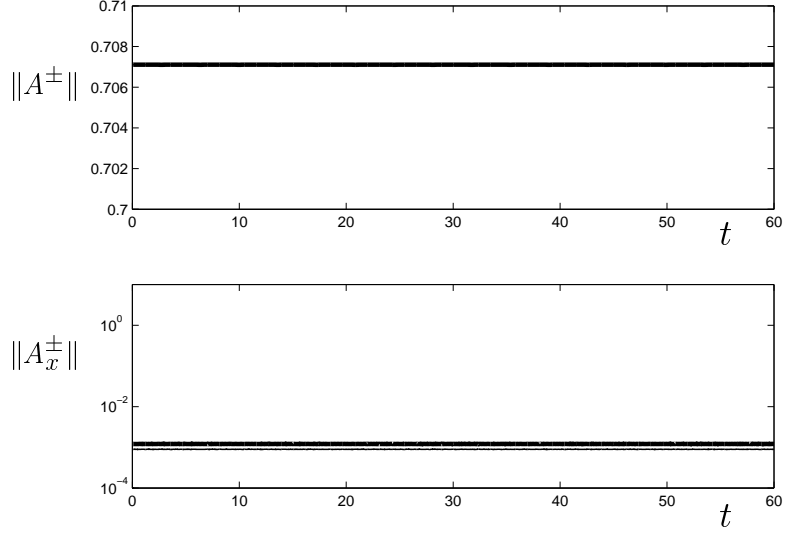


Figure 9: Thick (thin) lines indicate the time evolution of the spatial norm of A^+ (A^-) and its spatial derivative for $\kappa = 1$ and $\varepsilon = -10^{-3}$. The initial condition is the CW1 with a random perturbation of size $\sim 10^{-3}$ ($\sigma = \frac{1}{2}$).

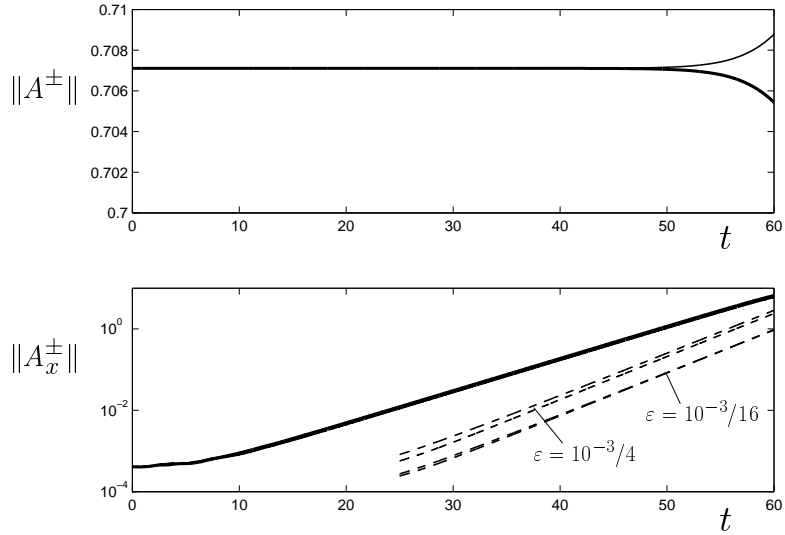


Figure 10: Thick (thin) lines indicate the time evolution of the spatial norm of A^+ (A^-) and its spatial derivative for $\kappa = 1$ and $\varepsilon = 10^{-3}$ (dashed lines correspond to smaller dispersion values). The initial condition is the CW1 with a random perturbation of size $\sim 10^{-3}$ ($\sigma = \frac{1}{2}$).

values; again, as predicted by the linear stability theory, the dispersive instability exponent goes to a nonzero value as the dispersion coefficient is reduced. A space-time representation of the

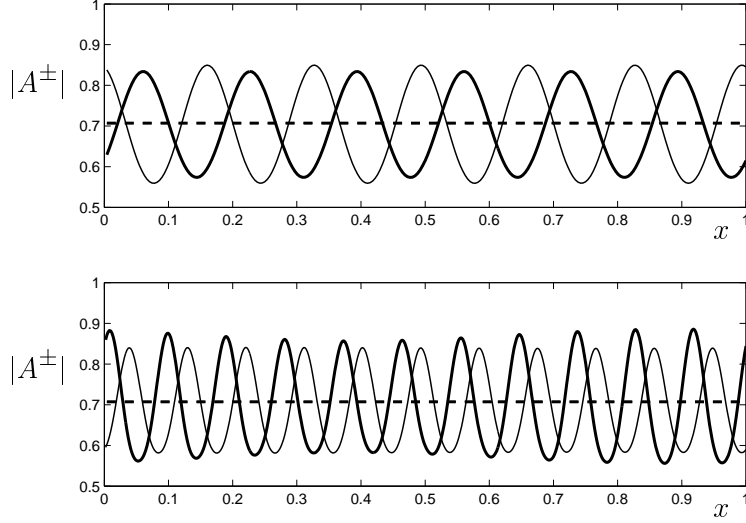


Figure 11: Snapshots of the solution of the NLCMEd at $t = 60$ ($|A^+|$:thick line, $|A^-|$:thin line), with parameters as in Fig. 10 and dispersion $\varepsilon = 10^{-3}$ (above) and $\varepsilon = 10^{-3}/4$ (below).

solution, once the dispersive scales are well developed, is presented in Fig.13 where it can be clearly appreciated that, in the short time scale $t \sim \sqrt{|\varepsilon|}$, the small dispersive scales are just transported by the group velocity but they also evolve on a slower time scale $t \sim 1$ producing a very complicated spatio-temporal pattern.

In conclusion, the main result of this paper is that the standard NLCME formulation fails to predict the system dynamics and that, in general, the small material dispersion terms should be taken into account, i.e., the NLCMEd eqs. (6)-(7) should be used, to appropriately describe the weakly nonlinear regime of light propagation in a FBG. In particular, the stability of the CW is seen to be drastically affected by dispersion. No matter how small is the dispersion or what sign it has, there are always stable CW according to the NLCME formulation that are dispersively unstable. The destabilization produced by the small dispersive terms is not a higher order, longer time effect; it takes place in the time scale of the NLCME and the associated growth rates remain of order one as the dispersion coefficient goes to zero. Once the dispersive scales are destabilized, they typically spread all over the domain producing a very complicated spatio-temporal dynamics (see Fig. 13) that is not captured by the NLCME. This behavior is the result of the competition of two effects with different asymptotic order: the dominating advection due to the group velocity and the dispersion. This situation generically arises in any extended propagative system with spatial reflection symmetry unless some special care is taken to reduce the group velocity. It has been

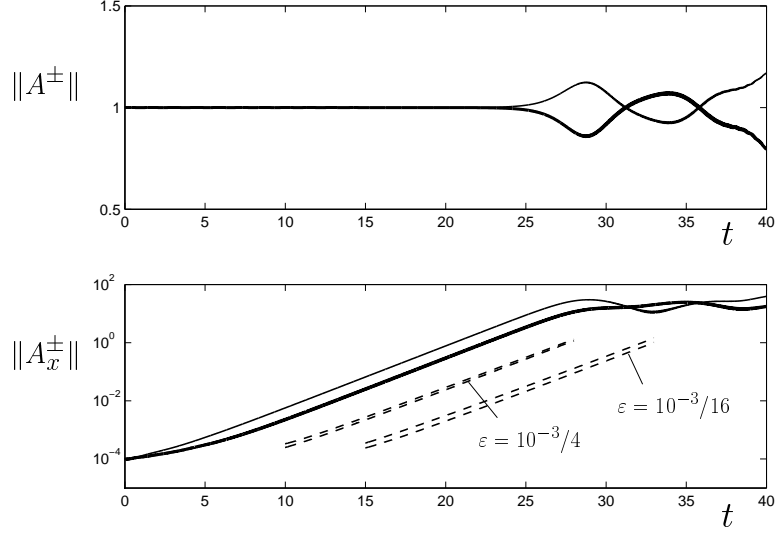


Figure 12: Thick (thin) lines indicate the time evolution of the spatial norm of A^+ (A^-) and its spatial derivative for $\kappa = 2$ and $\varepsilon = -10^{-3}$ (dashed lines correspond to smaller dispersion values). The initial condition is the CW2 with a random perturbation of size $\sim 10^{-3}$ ($\sigma = \frac{1}{2}$).

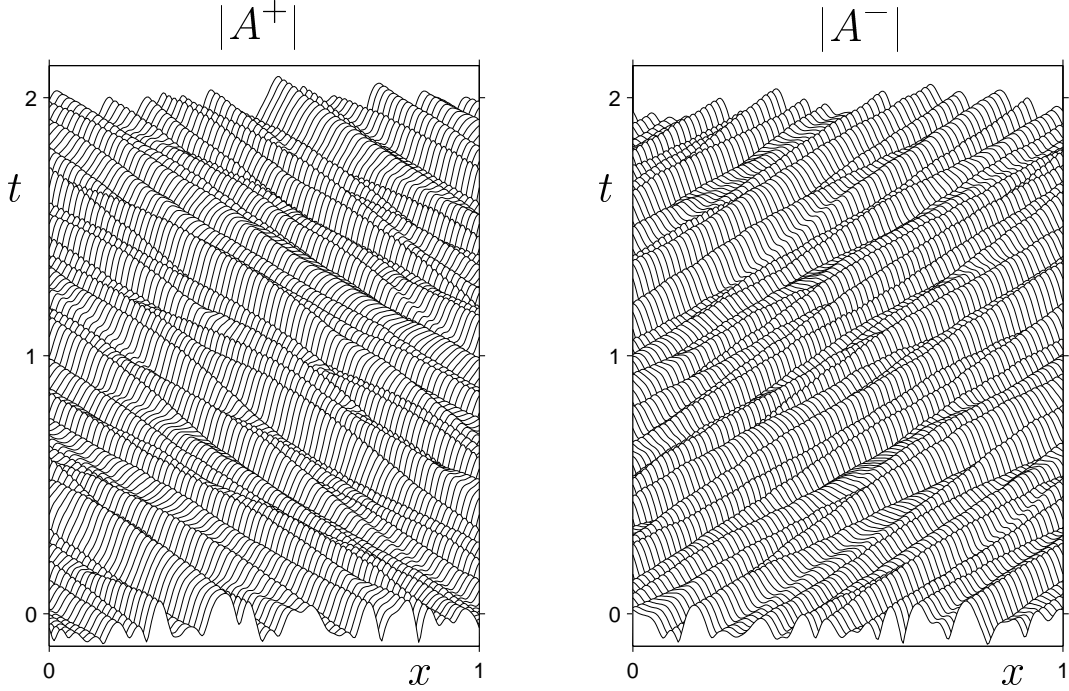


Figure 13: Space-time representation of the solution in Fig. 12 for two time units after $t = 80$.

previously found in the description of double Hopf bifurcation in dissipative systems [17, 18] and in parametrically forced surface waves [19].

There still remains the question of whether one should retain in the envelope equations more terms of the form $\pm\alpha\varepsilon^2 A_{xxx}^\pm$, $i\beta\varepsilon^3 A_{xxxx}^\pm, \dots$ and check if they produce new instabilities at even higher wavenumbers $k \sim |\varepsilon|^{-2/3}, |\varepsilon|^{-3/4}, \dots \gg |\varepsilon|^{-1/2}$. This is not necessary as it can be readily seen as follows. The two first dominant effects in the evolution of these very short wavelength perturbations are transport and dispersion and, proceeding as in section 4, they can be written as

$$A_k^\pm(t) e^{\pm ikt + i\varepsilon k^2 t + ikx}.$$

But, because of the effect of the dispersion, there is no possible coupling between A_k^\pm with $\overline{A_{-k}^\pm}$, which is no longer resonant, and hence there is no possible exponential instability (see eqs. (24) and (25)) at these higher wavenumbers.

As a final remark, it is interesting to mention that there are several recent rigorous proofs [6, 20] that establish that the solutions of the NLCME remain asymptotically close to solutions of the original physical equations. These proximity results are not in contradiction with the results of this paper because these proofs do not say anything about the stability of the solutions. Therefore, when a stable NLCME solution is dispersively unstable, its corresponding close solution of the physical equations is also unstable and the system likes to move away from this solution and develops dispersive scales, as the NLCME correctly predict.

Acknowledgments

The author would like to thank Carlos M. Casas for his help with the numerical simulations presented in this paper. This work was supported by the European Office of Aerospace Research and Development under contract FA8655-02-M4087 and by the Spanish Dirección General de Investigación under grant MTM2004-03808.

-
- [1] R. Kashyap, *Fiber Bragg Gratings*, Optics and Photonics (Academic Press, 1999).
 - [2] C. de Sterke and J. Sipe, Progress in Optics **XXXIII**, 203 (1994).
 - [3] A. Aceves, CHAOS **10**, 584 (2000).

- [4] Y. S. Kivshar and G. P. Agrawal, *Optical Solitons. From fibers to photonic crystals* (Academic Press, 2003).
- [5] H. Winful and G. Cooperman, Appl. Phys. Lett. **40**, 298 (1982).
- [6] R. Goodman, M. Weinstein, and P. Holmes, J. Nonlinear Sci. **11**, 123 (2001).
- [7] A. Yulin and D. Skryabin, Phys. Rev. E **67**, 023611 (2003).
- [8] H. Sakaguchi and B. Malomed, J. Phys. B: At. Mol. Opt. Phys. **37**, 1443 (2004).
- [9] A. Hasegawa, *Optical Solitons in Fibers* (Springer Verlag, 1990), 2nd ed.
- [10] M. Cross and P. Hohenberg, Rev. Mod. Phys. **65**, 851 (1993).
- [11] W. Mak, B. Malomed, and P. Chu, Phys. Rev. E **68**, 026609 (2003).
- [12] A. Champneys, B. Malomed, and M. Friedman, Phys. rev. Lett. **80**, 4169 (1998).
- [13] A. Champneys and B. Malomed, J. Phys. A: Math. Gen. **32**, L547 (1999).
- [14] J. Schöllmann and A. Mayer, Phys. Rev. E **61**, 5830 (2000).
- [15] C. de Sterke, J. Opt. Soc. Am. B **15**, 2660 (1998).
- [16] C. Canuto, H. Hussani, A. Quarteroni, and T. Zang, *Spectral Methods in Fluid Mechanics*, Springer Series in Computational Physics (Springer-Verlag, 1988).
- [17] C. Martel and J. Vega, Nonlinearity **9**, 1129 (1996).
- [18] C. Martel and J. Vega, Nonlinearity **11**, 105 (1998).
- [19] C. Martel, J. Vega, and E. Knoboch, Physica D **174**, 198 (2003).
- [20] G. Schneider and H. Uecker, Asymptot. Anal. **28**, 163 (2001).